

# Fokker–Planck approximation of the master equation in molecular biology

Paul Sjöberg · Per Lötstedt · Johan Elf

Received: 23 December 2005 / Accepted: 24 July 2006 / Published online: 16 February 2007  
© Springer-Verlag 2007

**Abstract** The master equation of chemical reactions is solved by first approximating it by the Fokker–Planck equation. Then this equation is discretized in the state space and time by a finite volume method. The difference between the solution of the master equation and the discretized Fokker–Planck equation is analyzed. The solution of the Fokker–Planck equation is compared to the solution of the master equation obtained with Gillespie’s Stochastic Simulation Algorithm (SSA) for problems of interest in the regulation of cell processes. The time dependent and steady state solutions are computed and for equal accuracy in the solutions, the Fokker–Planck approach is more efficient than SSA for low dimensional problems and high accuracy.

**Keywords** Master equation · Fokker–Planck equation · Numerical solution · Stochastic simulation algorithm

---

Communicated by G. Wittum.

---

P. Sjöberg · P. Lötstedt (✉)  
Division of Scientific Computing,  
Department of Information Technology,  
Uppsala University, P.O. Box 337, 75105 Uppsala, Sweden  
e-mail: perl@it.uu.se

J. Elf  
Department of Cell and Molecular Biology,  
Uppsala University, P.O. Box 596, 751 24 Uppsala, Sweden

*Present Address:*  
J. Elf  
Department of Chemistry and Biology, Harvard University,  
Cambridge, MA 02138, USA

## 1 Introduction

Biological cells are microscopical chemical reactors. They control their internal state through a complex regulatory network of non-equilibrium chemical reactions. The intracellular rules for chemistry is quite different from the circumstances when the descriptions of ordinary test tube chemistry applies. For one thing there is an enormous number of different reactants but only very few molecules of each kind. To gain understanding of the principles that is used in cells to control essential processes, it is therefore necessary to study drastically simplified models.

The validity of some assumptions of macroscopic kinetic modeling must be reinvestigated before they can be safely applied to biochemical systems in vivo. Sometimes the validity does not hold. In particular it has been widely appreciated that stochastic models for the dynamics of biochemical reactants are sometimes necessary replacements for the standard reaction rate equations which only apply strictly to mean values in infinitely large, yet, well stirred systems [21, 22].

The reaction rate equations will give an insufficient description of biochemical systems because molecule copy numbers are sometimes small [2, 3, 27], and because the molecules have a hard time finding and leaving each other due to slow intracellular diffusion [4, 9]. Biological macromolecules may also have many internal states which makes the individual reaction events more interesting than interactions between ions in dilute solutions [30].

The master equation is a scalar differential-difference equation for the time evolution of the probability density function (PDF) of the copy numbers of the molecular species participating in the molecular system [13, 22].

This equation is an accurate model on the meso scale of biochemical systems with small copy numbers. The number of space dimensions in the equation is  $N$ , where  $N$  is the number of different molecular species. When  $N$  is large, numerical solution of the master equation suffers from the “curse of dimensionality”. Suppose that the computational space is restricted to  $M_m$  points in every dimension. The computational work and memory requirements are then proportional to  $M_m^N$ , an exponential growth in  $N$ .

Gillespie has developed the Stochastic Simulation Algorithm (SSA), which is a Monte Carlo method for simulation of the trajectories of the molecular system in time [16]. By collecting statistics from the simulation, the PDF of the copy numbers is obtained approximately. The work grows linearly with  $N$ , making it possible to use this method also for large  $N$ . This method is the standard method for stochastic simulation of reaction networks in cells. A disadvantage is that many trajectories are needed for an accurate estimation of the time-dependent solution of the master equation and only long time-integrations yield accurate results for its steady state solution.

The master equation is approximated by a discretization of the Fokker–Planck equation (FPE) [13,22] on a Cartesian grid in this paper. The FPE is a time-dependent partial differential equation and it is discretized with a finite volume scheme as in [11]. The “curse of dimensionality” is an obstacle also for the numerical solution of the FPE but the number of grid points can be reduced dramatically compared to the master equation. If the number of points is  $M_{FP}$  in each dimension, then  $M_{FP} < M_m$  and  $M_{FP}^N \ll M_m^N$ . The difference between the solutions of the master equation and the discretized FPE is estimated by a maximum principle thanks to the parabolic nature of the FPE. This difference is quantified in numerical experiments.

The solution of the FPE is computed with a certain estimated accuracy and the solution of the master equation is determined by SSA with the same estimated accuracy. Problems with two, three, and four species are solved to different accuracies and the computing time is compared between the methods. In two dimensions, solution of the FPE is the preferred method, especially for higher accuracy. In many dimensions, SSA is the superior alternative. A theoretical support for this result is derived.

The paper is organized as follows. In the next section, the FPE is discretized in space and time. The PDF is determined by the SSA in Sect. 3 and the number of necessary realizations is discussed. The estimate of the difference between the solutions of the master equation and the discretized FPE is derived in Sect. 4. The FPE is

applied to four different molecular systems of biological interest described in Sect. 5 and compared to simulations with Gillespie’s algorithm in the last section. A vector is denoted by  $\mathbf{x}$  in bold and its  $j$ :th component by  $x_j$  in the sequel.

## 2 Deterministic solution of the Fokker–Planck equation

The FPE is derived from the master equation in this section following [22]. The FPE is then discretized in space and integrated by an implicit time-stepping scheme.

### 2.1 The FPE and its boundary conditions

Assume that we have a reaction with a transition from state  $\mathbf{x}_r$  to state  $\mathbf{x}$ . The vectors  $\mathbf{x}_r$  and  $\mathbf{x}$  have  $N$  non-negative integer components such that  $\mathbf{x}, \mathbf{x}_r \in \mathbb{Z}_+^N$  where  $\mathbb{Z}_+ = \{0, 1, 2, \dots\}$ . Each reaction can be described by a step  $\mathbf{n}_r$  and the probability flow from  $\mathbf{x}_r$  to  $\mathbf{x}$  by the rate  $w_r(\mathbf{x}_r)$

$$\mathbf{x}_r \xrightarrow{w_r(\mathbf{x}_r)} \mathbf{x}, \quad \mathbf{n}_r = \mathbf{x}_r - \mathbf{x}. \quad (1)$$

Let  $\partial_t$  denote the time derivative  $\partial/\partial t$ . The master equation corresponding to  $R$  reactions satisfied by the probability  $p$  to be in state  $\mathbf{x}$  at time  $t$  is

$$\Gamma_m(p) \equiv \partial_t p(\mathbf{x}, t) - \left( \sum_{\substack{r=1 \\ (\mathbf{x} + \mathbf{n}_r) \in \mathbb{Z}_+^N}}^R q_r(\mathbf{x} + \mathbf{n}_r, t) - \sum_{\substack{r=1 \\ (\mathbf{x} - \mathbf{n}_r) \in \mathbb{Z}_+^N}}^R q_r(\mathbf{x}, t) \right) = 0, \quad (2)$$

where  $q_r(\mathbf{x}, t) = w_r(\mathbf{x})p(\mathbf{x}, t)$ , see chapter 7.5 in [13]. A term is included in the first sum only if  $\mathbf{x} + \mathbf{n}_r$  is a possible state and in the second sum only if  $\mathbf{x}$  can be reached from a possible state by the reaction.

The FPE is derived from (2) by Taylor expansion around  $\mathbf{x}$  (the Kramers–Moyal expansion) and ignoring terms of order three and higher, see [10,22]. Let  $\mathbf{x} = (x_1, x_2, \dots, x_N)^T \in \mathbb{R}_+^N = \{\mathbf{x} \mid x_i \geq 0, i = 1, \dots, N\}$  and

let  $\partial_i$  denote the space derivative  $\partial/\partial x_i$ . Then we have

$$G(p) \equiv \partial_t p(\mathbf{x}, t) - \sum_{r=1}^R \left( \sum_{i=1}^N n_{ri} \partial_i q_r(\mathbf{x}, t) + \frac{1}{2} \sum_{i=1}^N \sum_{j=1}^N n_{ri} n_{rj} \partial_i \partial_j q_r(\mathbf{x}, t) \right) = 0. \tag{3}$$

The FPE is written in conservation form by introducing  $\mathbf{F}_r$  with the components

$$F_{ri} = n_{ri} \left( q_r + \frac{1}{2} \mathbf{n}_r \cdot \nabla q_r \right), \quad r = 1, \dots, R, \quad i = 1, \dots, N.$$

Then by (3)

$$\partial_t p(\mathbf{x}, t) = \sum_{r=1}^R \nabla \cdot \mathbf{F}_r. \tag{4}$$

Integrate (4) over a computational cell  $\omega$  with boundary  $\partial\omega$  and boundary normal  $\hat{\mathbf{n}}_\omega$  and apply Gauss' formula to obtain

$$\begin{aligned} \partial_t \int_\omega p(\mathbf{x}, t) d\omega &= \int_\omega \partial_t p d\omega = \int_\omega \nabla \cdot \sum_{r=1}^R \mathbf{F}_r d\omega \\ &= \int_{\partial\omega} \sum_{r=1}^R \mathbf{F}_r \cdot \hat{\mathbf{n}}_\omega ds. \end{aligned} \tag{5}$$

This is the basis for the finite volume discretization.

Assume that we are interested in the solution in a multidimensional cube  $\Omega \subset \mathbb{R}_+^N$  with the boundary

$$\partial\Omega = \cup_{j=1}^N \partial\Omega_j, \quad \partial\Omega_j = \{\mathbf{x} \mid x_j = 0 \vee x_j = x_{j,\max} > 0\}.$$

By letting  $\mathcal{F} = \sum_{r=1}^R \mathbf{F}_r$  and assuming reflecting boundary conditions on  $\partial\Omega$ , i.e. particles cannot leave the region [13], we have that  $\mathcal{F}_j = 0$  on  $\partial\Omega_j$ . It follows from [11] that the total probability

$$\mathcal{P}(t) = \int_\Omega p(\mathbf{x}, t) d\Omega$$

is constant for  $t \geq 0$ .

### 2.2 Space discretization

A Cartesian computational grid is generated so that in 2D the computational domain  $\Omega_h$  defined by  $[0, x_{1,\max}] \times [0, x_{2,\max}]$  is covered by the rectangular cells  $\omega_{ij}$ ,  $i = 1, \dots, M_1$ ,  $j = 1, \dots, M_2$ , of length  $h_i^x$  in the  $x$ -direction and  $h_j^y$  in the  $y$ -direction and with midpoints at  $\mathbf{x}_{ij} = (x_i, y_j)$ . At  $i = 1$  we have  $\mathbf{x}_{1j} = (h_1^x/2, y_j)$  and  $\mathbf{x}_{i1} = (x_i, h_1^y/2)$  at  $j = 1$ . The rightmost midpoints  $\mathbf{x}_{M_1,j}$  and  $\mathbf{x}_{i,M_2}$  are chosen such that the solution  $p$  can be

approximated by zero at the outer boundary of  $\Omega_h$  at  $(x_{M_1} + h_{M_1}^x/2, y_j)$ ,  $j = 1, \dots, M_2$ , and  $(x_i, y_{M_2} + h_{M_2}^y/2)$ ,  $i = 1, \dots, M_1$ .

From (5) we have for the average  $p_{ij}$  of  $p$  in  $\omega_{ij}$  with area  $|\omega_{ij}| = h_i^x h_j^y$

$$\partial_t p_{ij} = \frac{1}{|\omega_{ij}|} \int_{\partial\omega_{ij}} \mathcal{F} \cdot \hat{\mathbf{n}}_\omega ds. \tag{6}$$

For evaluation of the integral on  $\partial\omega_{ij}$ , we need an approximation of

$$\mathcal{F} = \sum_{r=1}^R \mathbf{n}_r \left( q_r + \frac{1}{2} \mathbf{n}_r \cdot \nabla q_r \right) \tag{7}$$

using the cell averages  $p_{ij}$ . With a centered approximation of  $\sum_{r=1}^R n_{ri} q_r$  we have on the face  $(i+1/2, j)$  between  $\omega_{ij}$  and  $\omega_{i+1,j}$

$$\sum_{r=1}^R n_{ri} q_r = \frac{1}{2} (w_{i+1,j} p_{i+1,j} + w_{ij} p_{ij}), \tag{8}$$

where  $w_{ij} = \sum_{r=1}^R n_{ri} w_r(x_{ij})$ .

A shifted dual cell  $\omega_{i+1/2,j}$  is introduced. The midpoint of  $\omega_{ij}$  is located on the left hand face of  $\omega_{i+1/2,j}$  and the midpoint of  $\omega_{i+1,j}$  on the right hand face. The gradient in the dual cell is computed using Gauss' theorem

$$\begin{aligned} \nabla q_{i+1/2,j} &= \frac{1}{|\omega_{i+1/2,j}|} \int_{\omega_{i+1/2,j}} \nabla q d\omega \\ &= \frac{1}{|\omega_{i+1/2,j}|} \int_{\partial\omega_{i+1/2,j}} q \hat{\mathbf{n}}_\omega ds. \end{aligned} \tag{9}$$

Then  $q$  is approximated at the right hand face of  $\omega_{i+1/2,j}$  by  $q_{i+1,j}$ , at the left hand face by  $q_{ij}$ , at the upper face by  $(q_{i+1,j+1} + q_{i+1,j} + q_{i,j+1} + q_{ij})/4$  and at the lower face by  $(q_{i+1,j-1} + q_{i+1,j} + q_{i,j-1} + q_{ij})/4$ . The approximation on the other cell faces of  $\omega_{ij}$  follows the same idea. The flux  $\mathcal{F}$  in (7) can now be computed on all cell faces using (8) and (9). The scheme is second order accurate on grids with constant grid size.

The space discretization can be summarized in 2D by

$$\begin{aligned} \frac{dp_{ij}}{dt} &= (h_i^x)^{-1} (\mathcal{F}_{1,i+1/2,j} - \mathcal{F}_{1,i-1/2,j}) \\ &\quad + (h_j^y)^{-1} (\mathcal{F}_{2,i,j+1/2} - \mathcal{F}_{2,i,j-1/2}), \\ &\quad i = 1, \dots, M_1, \quad j = 1, \dots, M_2. \end{aligned} \tag{10}$$

Since at most two dimensions are involved in the derivatives in (3), the generalization of (10) to more dimensions than two is relatively straightforward.

After space discretization and with the vector  $\mathbf{p}$  containing the unknown cell averages of length  $M = \prod_{i=1}^N$

$M_i$ , the FPE approximation is

$$\frac{d\mathbf{p}}{dt} = A\mathbf{p}, \quad (11)$$

where  $A \in \mathbb{R}^{M \times M}$  is a constant, very sparse matrix. It is proved in [11] that  $A$  has one eigenvalue equal to zero when the discretization is conservative as in (10). When  $N$  grows,  $M$  increases exponentially fast. This is the ‘‘curse of dimensionality’’ but the growth is slower for the FPE with  $h_i > 1$  than for the master equation.

### 2.3 Time discretization

We are interested in computing the steady state solution and the time dependent solution of (11).

The time integration is performed by the backward differentiation formula of second order, BDF-2 [18]. This method is implicit and stable if the real part of the eigenvalues  $\lambda(A)$  of  $A$ ,  $\Re\lambda(A)$ , is non-positive. There are different time scales in the dynamics of biological systems [7] favoring a method suitable for stiff equations where the time step can be selected with only the accuracy in mind. This is an advantage compared to SSA where stiff problems are advanced with small time steps determined by the fast time scale. Work is in progress trying to remedy this inefficiency of SSA, see e.g. [5, 19].

Let the time step between  $t^{n-1}$  and  $t^n$  be  $\Delta t^n$ . It is chosen adaptively according to [25] such that the local discretization error is smaller than a given tolerance  $\epsilon$ . Then the coefficients in the BDF scheme depend on the present and the previous time steps [18, 25]. The system of linear equations to solve for  $\mathbf{p}^n$  at each time step is

$$\begin{aligned} (\alpha_0^n I - \Delta t^n A)\mathbf{p}^n &= -\alpha_1^n \mathbf{p}^{n-1} - \alpha_2^n \mathbf{p}^{n-2} \\ \theta^n &= \Delta t^n / \Delta t^{n-1} \\ \alpha_0^n &= (1 + 2\theta^n) / (1 + \theta^n), \\ \alpha_1^n &= -(1 + \theta^n), \\ \alpha_2^n &= (\theta^n)^2 / (1 + \theta^n), \end{aligned} \quad (12)$$

where  $I \in \mathbb{R}^{M \times M}$  is the identity matrix.

The time-dependent solution  $\mathbf{p}^n$  in (12) is computed by an iterative method in every time step. We have chosen Bi-CGSTAB [29] with incomplete LU (ILU) preconditioning of  $A$  [17] for rapid convergence. The steady state solution  $\mathbf{p}^\infty$  of (11) satisfying

$$A\mathbf{p}^\infty = 0 \quad (13)$$

is determined by computing the eigenvector of  $A$  corresponding to  $\lambda(A) = 0$  with an Arnoldi method [24] or a Jacobi–Davidson method [28] for sparse, nonsymmetric matrices.

### 2.4 Error estimation

The error in the steady state solution of the FPE can be estimated by computing the solution for the same problem on a coarser grid and compare the two solutions. Let the solution be  $p_h$  of the FPE and  $p_{2h}$  the solution where the grid size is doubled in all dimensions. The solution on the fine grid is restricted to the coarse grid by the operator  $R_{2h}$  by taking the mean value of  $p_h$  in the fine cells corresponding to each coarse cell. The solution error  $e_h$  in  $p_h$  is then estimated for second order discretizations by

$$e_h = (R_{2h}p_h - p_{2h})/3.$$

An additional error in the time-dependent problem is due to the time discretization. The total solution error  $e_{h,k}$  in  $p_{h,k}$  at  $t = T$  with  $\Delta t = k$  is estimated by computing  $p_{2h,2k}$ , the coarse grid solution computed in every second time step of the fine grid solution. The estimate of  $e_{h,k}$  at  $T$  is

$$e_{h,k} = (R_{2h}p_{h,k} - p_{2h,2k})/3.$$

In  $N$  space dimensions, the computational work to calculate  $p_{2h}$  is reduced by a factor  $2^{-N}$  and to calculate  $p_{2h,2k}$  by  $2^{-(N+1)}$  compared to the work to determine  $p_h$  and  $p_{h,k}$ . Hence, the cost of the error estimates is low for the FPE.

The error is measured in the  $\ell_1$ -norm  $\|\cdot\|_1$  defined as follows. Let  $v = (v_1, \dots, v_N)$  be a multi-index with  $1 \leq v_j \leq M_j$  and  $|v| = \sum_{j=1}^N v_j$ , and let  $\omega_v$  be a cell in  $\Omega_h$ . For a scalar grid function  $f_v(t)$  we have

$$\|\mathbf{f}(t)\|_1 = \sum_v |\omega_v| |f_v(t)|. \quad (14)$$

### 2.5 Work to solve the FPE

Suppose that  $h$  is the step length in each dimension,  $\epsilon$  is the error tolerance, and that the discretization error is of order  $r$ . Then  $\epsilon \propto h^r$  and the size  $M$  of the discretized equation (11) satisfies  $M \propto h^{-N}$ . The number of non-zero elements in the stencil at one grid point is at most  $1 + 2N^2$ . If the work for finding the zero eigenvalue and its eigenvector is approximately proportional to  $M$ , the work to compute the steady state solution is

$$W(\epsilon) = C_s(N)\epsilon^{-\frac{N}{r}}, \quad (15)$$

where  $C_s$  is independent of  $\epsilon$ .

For the number of time steps  $K$ , we have  $K \propto (\Delta t)^{-1}$ . The work in each time step is proportional to  $M$  and the error tolerance  $\epsilon \propto (\Delta t)^r$  for an  $r$ :th order time

integrator. Thus, the total work is

$$W(\epsilon) = C_t(N)\epsilon^{-\frac{N+1}{r}}, \tag{16}$$

where  $C_t$  has the same property as  $C_s$ .

The memory requirements to store  $\mathbf{p}^{n-1}$  and  $\mathbf{p}^n$  is  $2M$  floating point numbers. Additional workspace in Bi-CGSTAB and the eigensolvers proportional to  $\gamma M$  is necessary. Here  $\gamma$  is 5 – 10.

The generation of the constant matrix  $A$  was implemented in C++ and imported into MATLAB [26] for time integration and computation of eigenpairs. The adaptive time integrator was implemented in MATLAB.

### 3 Monte Carlo solution of the master equation

The master equation is solved by Gillespie’s algorithm SSA [16]. The computational domain  $\Omega_h$  is partitioned into the same cells as in Sect. 2. Since  $h_i > 1$ , each cell contains many states of the state vector  $\mathbf{x}$ . The probability of the system to be in a cell is estimated from one trajectory in the steady state case assuming ergodicity and several trajectories in the time-dependent case. At least  $M$  floating point numbers have to be stored for the probabilities in the  $M$  cells.

#### 3.1 Steady state problem

The SSA generates one trajectory of the chemical system. The probability of the system to be in a cell  $v$  in a time interval  $\Delta\tau$  between  $\tau^{n-1}$  and  $\tau^n$  is denoted by  $P_v^n$ . It is computed as the quotient between the fraction of time  $\Delta\tau_v^n$  spent by the trajectory in the states in cell  $v$  in the interval  $(\tau^{n-1}, \tau^n]$  and  $\Delta\tau$

$$P_v^n = \Delta\tau_v^n / \Delta\tau.$$

After the transient, when the steady state solution is approached,  $P_v^n$ ,  $n = n_{tr} + 1, n_{tr} + 2, \dots$  are considered as a sequence of independent random variables in a stationary stochastic process. The average of  $P_v^n$  between  $n_{tr}$  and  $n_{tr} + \Delta n$ , defined by

$$\bar{P}_v^{\Delta n} = \frac{1}{\Delta n} \sum_{n=n_{tr}+1}^{n_{tr}+\Delta n} P_v^n, \tag{17}$$

is normally distributed  $\mathcal{N}(\mu_v, \sigma_v^2 / \Delta n)$  according to the central limit theorem [23]. The standard deviation of  $\bar{P}_v^{\Delta n}$  depends on the standard deviation  $\sigma_v$  of  $P_v^n$ . The steady state solution determined by the stochastic algorithm has an expected value  $\mu_v$  corresponding to the probability  $p_v^\infty$  in (13) computed by the FPE.

#### 3.2 Error estimation and computational work

The error in  $\bar{P}_v^{\Delta n}$  in cell  $v$  is  $e_v = \bar{P}_v^{\Delta n} - \mu_v$  and can be estimated by Student’s  $t$  distribution [23]. Let  $s_v^2$  be the sample variance defined by

$$s_v^2 = \frac{1}{m-1} \sum_{n=n_0+1}^{n_0+m} (P_v^n - \bar{P}_v^{\Delta n})^2,$$

for some  $n_0$ . The sample standard deviation of  $P_v^n$  is computed using  $m = 100$  samples in a separate simulation of the system. Then we have with probability 0.68

$$-s_v / \sqrt{\Delta n} \leq e_v \leq s_v / \sqrt{\Delta n}$$

and

$$\|\mathbf{e}\|_1 \lesssim \|\mathbf{s}\|_1 / \sqrt{\Delta n}. \tag{18}$$

A 95 % confidence interval would require a  $\Delta n$  about four times as large.

The length of  $\Delta\tau$  for a reliable  $s_v$  depends on the properties of the system. If  $\Delta\tau$  is too small, the sampling will be biased by the initial state of the simulation and  $\|\sigma\|_1$  will be underestimated. Numerical experiments are employed to determine a suitable  $\Delta\tau$  for each system by computing  $\|\mathbf{s}\|_1$  for increasing  $\Delta\tau$  until the estimates conform with what is expected from the central limit theorem. The variance is itself a stochastic variable having a  $\chi^2$ -distribution [23]. A 90% confidence interval for  $\sigma_v$  with  $m = 100$  is  $(0.896s_v, 1.134s_v)$ .

With the error tolerance  $\epsilon$ , the number of samples  $\Delta n$  of  $P_v^n$  after the transient follows from (18)

$$\Delta n \approx (\|\mathbf{s}\|_1 / \epsilon)^2.$$

The total simulation time  $T_{\max}$  will then be

$$T_{\max} = \Delta n \Delta\tau \approx \Delta\tau (\|\mathbf{s}\|_1 / \epsilon)^2. \tag{19}$$

The number of steps in SSA to reach  $T_{\max}$  is problem dependent but is independent of  $\epsilon$ . Compared to the error estimation for the FPE, computing  $\|\mathbf{s}\|_1$  for SSA is a relatively expensive operation, see the results in Sect. 6.

The SSA was implemented in C for each model system in Sect. 5 separately in order to avoid unnecessary efficiency losses associated with a more general implementation.

#### 3.3 The time-dependent problem

In order to compute the PDF  $p_v(T)$  at time  $T$ ,  $L$  different trajectories are generated by SSA up to  $t = T$ . Partition  $L$  into  $L_0$  intervals of length  $\Delta\lambda$ , introduce the number

of trajectories  $\Delta\lambda_v^l$  in the  $l$ :th interval in cell  $v$ , and define  $P_v^l(T) = \Delta\lambda_v^l / \Delta\lambda$ .

The result is a stochastic variable  $P_v^l(T)$ ,  $l = 1, \dots, L_0$ . An increasing  $l$  corresponds to an increasing time for the steady state problem. The average value

$$\bar{P}_v(T) = \frac{1}{L_0} \sum_{l=1}^{L_0} P_v^l(T) \quad (20)$$

is normally distributed  $\mathcal{N}(\mu_v(T), \sigma_v^2(T)/L_0)$ , cf. (17). The total number of necessary realizations for an error  $e_v(T)$  satisfying  $\|\mathbf{e}(T)\|_1 \approx \epsilon$  is

$$L \approx \Delta\lambda(\|\mathbf{s}\|_1/\epsilon)^2. \quad (21)$$

where  $\mathbf{s}$  is calculated as above. A suitable size of  $\Delta\lambda$  is problem dependent and is determined in the same way as  $\Delta\tau$ . The total work is proportional to  $L$  and therefore also to  $\epsilon^{-2}$ .

#### 4 Comparison of the solutions

The solution of the master equation is compared to the solution of the discretized FPE in this section and a bound on the difference is derived.

For a sufficiently smooth  $p$  we have for the difference between the FPE (3) and the master equation (2)

$$G(p) - \Gamma_m(p) = \tau_m(p). \quad (22)$$

The remainder term  $\tau_m$  consists of the truncated part of the Taylor expansions in space when the FPE is formed from the master equation. If  $p$  solves the FPE then  $G(p) = 0$  and

$$\Gamma_m(p) = -\tau_m(p).$$

A solution  $\hat{p}_m$  of the master equation defined at  $\mathbf{x} \in \mathbb{Z}_+^N$  is extended by a smooth reconstruction  $p_m$  to  $\mathbf{x} \in \mathbb{R}_+^N$ , e.g. by a polynomial approximation. Then we have  $\hat{p}_m(\mathbf{x}) = p_m(\mathbf{x})$  for  $\mathbf{x} \in \mathbb{Z}_+^N$  so that

$$G(p_m) = \tau_m(p_m) + \Gamma_m(p_m), \quad (23)$$

and at the non-negative integer points  $\Gamma_m(p_m) = 0$ .

In the same manner, let  $\hat{p}_{FP}$  be the solution of the discretized FPE according to (12) so that  $\Gamma_{FP}(\hat{p}_{FP}) = 0$  at  $t^n$ ,  $n = 0, 1, \dots$ , and at e.g. the midpoints of the cells. Extend  $\hat{p}_{FP}$  smoothly to  $p_{FP}$  defined for  $t > 0$ ,  $\mathbf{x} \in \mathbb{R}_+^N$ . The difference between  $G$  and  $\Gamma_{FP}$  for a sufficiently smooth  $p$  is

$$G(p) - \Gamma_{FP}(p) = \tau_{FP}(p), \quad (24)$$

where  $\tau_{FP}$  is the discretization or truncation error when  $G$  is approximated by  $\Gamma_{FP}$ . If  $p$  solves the FPE, then

we have

$$\Gamma_{FP}(p) = -\tau_{FP}(p).$$

For  $p_{FP}$  we have

$$G(p_{FP}) = \tau_{FP}(p_{FP}) + \Gamma_{FP}(p_{FP}), \quad (25)$$

and at the midpoints  $\Gamma_{FP}(p_{FP}) = 0$ . Since  $G$  is linear in  $p$  in (3) we can subtract (23) from (25) to obtain

$$\begin{aligned} G(p_{FP} - p_m) &= G(p_{FP}) - G(p_m) = \varepsilon(p_{FP}, p_m), \\ \varepsilon(p_{FP}, p_m) &= \tau_{FP}(p_{FP}) - \tau_m(p_m) \\ &\quad + \Gamma_{FP}(p_{FP}) - \Gamma_m(p_m). \end{aligned} \quad (26)$$

The difference  $\delta p$  between the reconstructed solutions  $p_{FP}$  and  $p_m$  of the master equation and the discretized FPE satisfies a FPE with a small driving right hand side  $\varepsilon$ . The right hand side can be estimated by higher derivatives of  $p_{FP}$  and  $p_m$  and bounds on  $\Gamma_{FP}$  and  $\Gamma_m$ . A bound on  $\delta p$  depending on  $\mathbf{n}_r$ ,  $w_r$ ,  $r = 1, \dots, R$ , the deviation of  $\Gamma_{FP}$  and  $\Gamma_m$  from zero,  $\tau_{FP}$  and  $\tau_m$  will now be derived.

First we need the definitions of a few norms for a scalar  $f(\mathbf{x}, t)$  with  $\mathbf{x} \in \Omega \subset \mathbb{R}_+^N$  and  $t \in \mathcal{T} = [0, T]$  and a vector  $\mathbf{x}$ :

$$|f|_\infty = \sup_{\Omega, \mathcal{T}} |f(\mathbf{x}, t)|, \quad \|\mathbf{x}\|_2^2 = \mathbf{x}^T \mathbf{x},$$

$$\|D^{(\alpha)} f\|_\infty = \max_{|\nu|=\alpha} |\partial_{v_1} \partial_{v_2} \dots \partial_{v_N} f(\mathbf{x}, t)|_\infty.$$

The first lemma provides bounds on  $\tau_m$  and  $\tau_{FP}$ .

**Lemma 1** Assume that  $p_m \in C^3$  and  $p_{FP} \in C^4$  and that  $\mathbf{n}_r$  is bounded for all  $r$  and let  $q_{rm} = w_r p_m$  and  $q_{rFP} = w_r p_{FP}$ . The difference  $\tau_m$  in (22) is bounded by

$$|\tau_m(p_m)|_\infty \leq c_m \max_r \|D^{(3)} q_{rm}\|_\infty.$$

The discretization error  $\tau_{FP}$  in (24) is bounded by

$$\begin{aligned} |\tau_{FP}(p_{FP})|_\infty &\leq \frac{1}{3} \Delta t^2 |\partial_t^3 p_{FP}|_\infty + c_s h^2 (\max_r \|D^{(3)} q_{rFP}\|_\infty \\ &\quad + \max_r \|D^{(4)} q_{rFP}\|_\infty), \end{aligned}$$

where  $h$  is the maximum grid size.

*Proof* The remainder term  $\rho_r$  after the first two terms in the Taylor expansion of  $q_r(\mathbf{x} + \mathbf{n}_r) - q_r(\mathbf{x})$  is

$$\begin{aligned} \rho_r(q_r) &= q_r(\mathbf{x} + \mathbf{n}_r) - q_r(\mathbf{x}) \\ &\quad - \sum_i n_{ri} \partial_i q_r - 0.5 \sum_{i,j} n_{ri} n_{rj} \partial_i \partial_j q_r \\ &= \frac{1}{6} \sum_{i,j,k} n_{ri} n_{rj} n_{rk} \int_0^1 \partial_i \partial_j \partial_k q_r(\mathbf{x} + \zeta \mathbf{n}_r) d\zeta, \end{aligned}$$

see [6]. Since

$$\tau_m(p_m) = \sum_{r=1}^R \rho_r(q_{rm}),$$

it follows that there is a  $c_m$  depending on  $\mathbf{n}_r$  such that the first inequality holds.

The discretization error or remainder term in the Taylor expansion  $\tau_{\text{FP}t}$  due to the time discretization in (12) is bounded by (see [18])

$$|\tau_{\text{FP}t}| \leq \frac{1}{3} \Delta t^2 \sup_T |\partial_t^3 p_{\text{FP}}|.$$

The error in the space discretization  $\tau_{\text{FP}s}$  due to the first and second derivatives is in the same way bounded by

$$|\tau_{\text{FP}s}|_\infty \leq c_s h^2 (\max_r \|D^{(3)} q_{r\text{FP}}\|_\infty + \max_r \|D^{(4)} q_{r\text{FP}}\|_\infty)$$

for some positive  $c_s$ . The lemma is proved.  $\square$

The second lemma is needed to show that the coefficients in front of the second derivatives in the FPE (3) are positive definite under certain conditions. The stoichiometric matrix  $S$  of the reactions is defined by

$$S = (\mathbf{n}_1, \mathbf{n}_2, \dots, \mathbf{n}_R) \in \mathbb{R}^{N \times R}. \tag{27}$$

**Lemma 2** Assume that the rank of the stoichiometric matrix  $S$  in (27) is  $N$  and that  $w_r(\mathbf{x}) \geq w_0 > 0$  in a domain  $\Omega$  for every  $r$ . Then

$$\mathbf{p}^T \left( \sum_{r=1}^R w_r \mathbf{n}_r \mathbf{n}_r^T \right) \mathbf{p} \geq w_0 \mathbf{p}^T \mathbf{p}.$$

*Proof* The matrix  $\mathbf{n}_r \mathbf{n}_r^T$  has one eigenvalue  $\lambda_r = \mathbf{n}_r^T \mathbf{n}_r$  different from zero and the corresponding eigenvector is  $\mathbf{n}_r$ . There is no  $\mathbf{p} \neq 0$  such that  $\mathbf{n}_r^T \mathbf{p} = 0$  for all  $r$  since  $\mathbf{n}_r, r = 1, \dots, R$ , span  $\mathbb{R}^N$ . A lower bound on the sum  $\sum_{r=1}^R w_r (\mathbf{n}_r^T \mathbf{p})^2$  is given by a  $\mathbf{p} = \alpha \mathbf{n}_j$  such that  $w_j \lambda_j^2$  is minimal

$$\sum_{r=1}^R w_r \alpha^2 (\mathbf{n}_r^T \mathbf{n}_j)^2 \geq \alpha^2 w_j (\mathbf{n}_j^T \mathbf{n}_j)^2 = w_j \|\mathbf{n}_j\|_2^2 \mathbf{p}^T \mathbf{p} \geq w_0 \mathbf{p}^T \mathbf{p},$$

since  $\|\mathbf{n}_j\|_2^2 \geq 1$ .  $\square$

We are now prepared to prove an upper bound on the difference  $\delta p$  between one function  $p_{\text{FP}}$  interpolating the solution of the discretized FPE and one function  $p_m$  interpolating the solution of the master equation. The proof is based on the maximum principle for parabolic partial differential equations. The difference will satisfy (26) in a weak sense, i.e. for any smooth function

$\phi(\mathbf{x}, t)$  with compact support we have

$$\int_T \int_\Omega \phi(G(\delta p) - \varepsilon) \, d\mathbf{x} \, dt = 0.$$

For a discussion of weak solutions of partial differential equations, see e.g. [1, 20].

**Theorem** Assume that the stoichiometric matrix  $S$  and the propensities  $w_r$  satisfy the conditions in Lemma 2 in  $\Omega$  and that  $|w_r|, |\partial_{x_i} w_r|, |\partial_i \partial_j w_r|$ , and  $\mathbf{n}_r$  are bounded for all  $r, i$ , and  $j$  in  $\Omega$ . Furthermore, assume that on the boundary  $\partial\Omega$  of  $\Omega$  we have  $|(p_{\text{FP}} - p_m)(\mathbf{x}, t)| \leq \epsilon$  for the reconstructed solutions  $p_m \in C^3$  and  $p_{\text{FP}} \in C^4$ . Then

$$|(p_{\text{FP}} - p_m)(\mathbf{x}, t)| \leq \epsilon + C(\epsilon d + \mu),$$

where  $\mu$  is defined by

$$|\varepsilon(p_m, p_{\text{FP}})|_\infty \leq \mu = |\Gamma_{\text{FP}}(p_{\text{FP}})|_\infty + |\Gamma_m(p_m)|_\infty + |\tau_m(p_m)|_\infty + |\tau_{\text{FP}}(p_{\text{FP}})|_\infty.$$

Here,  $C$  and  $d$  depend on  $w_0, T$ , the size of  $\Omega$ , the bounds on  $w_r$  and its first and second derivatives, and the bound on  $\mathbf{n}_r$ . The discretization errors  $\tau_m$  and  $\tau_{\text{FP}}$  are bounded in Lemma 1.

*Proof* Let

$$\begin{aligned} \nabla \cdot \mathcal{A}(p, \nabla p) &= 0.5 \sum_r \sum_{i,j} \partial_i (w_r n_{ri} n_{rj} \partial_j p), \\ \mathcal{B}(p, \nabla p) &= \sum_r \sum_i n_{ri} (\omega_r \partial_i p + p \partial_i \omega_r), \\ \omega_r &= w_r + 0.5 \sum_j n_{rj} \partial_j w_r. \end{aligned}$$

Then the FPE (3) can be written

$$G(p) = \partial_t p - (\nabla \cdot \mathcal{A}(p, \nabla p) + \mathcal{B}(p, \nabla p)) = 0,$$

and it follows from Lemma 2 that

$$\begin{aligned} \mathbf{q} \cdot \mathcal{A}(p, \mathbf{q}) &= 0.5 \sum_r \sum_{i,j} q_i (w_r n_{ri} n_{rj} q_j) \\ &= 0.5 \sum_r w_r \sum_i q_i n_{ri} \sum_j q_j n_{rj} \\ &= 0.5 \sum_r w_r (\mathbf{q}^T \mathbf{n}_r)^2 \geq 0.5 w_0 \mathbf{q}^T \mathbf{q}. \end{aligned}$$

There is a bound on  $\mathcal{A}(p, \mathbf{q})$  with a function  $f_q(\mathbf{x}, t)$  such that

$$\|\mathcal{A}(p, \mathbf{q})\|_2 \leq f_q \|\mathbf{q}\|_2.$$

Moreover, there are functions  $g_p(\mathbf{x}, t)$  and  $g_q(\mathbf{x}, t)$  such that

$$|\mathcal{B}(p, \mathbf{q})| \leq g_p |p| + g_q \|\mathbf{q}\|_2.$$

Since  $\mathbf{n}_r$  and  $w_r, \partial_i w_r, \partial_i \partial_j w_r$ , are all bounded in  $\Omega$ , there are bounds on  $f_q, g_p$ , and  $g_q$

$$|f_q|_\infty = e, |g_p|_\infty = d, |g_q|_\infty = c.$$

By Lemma 1 we have a bound on  $|\tau_{\text{FP}} - \tau_m|_\infty \leq |\tau_{\text{FP}}|_\infty + |\tau_m|_\infty$ . Then the estimate

$$p_{\text{FP}} - p_m \leq \epsilon + C(\epsilon d + \mu)$$

follows from the maximum principle with  $p = q = \infty$  in Theorem 1 in [1]. The lower bound on  $\delta p$

$$-\epsilon - C(\epsilon d + \mu) \leq p_{\text{FP}} - p_m$$

is obtained by applying the same theorem to the equation for  $p_m - p_{\text{FP}}$ .  $\square$

*Remark* Under certain conditions, a similar bound can be derived for the difference between the steady state solutions  $p_{\text{FP}}(\mathbf{x})$  and  $p_m(\mathbf{x})$  following [15].

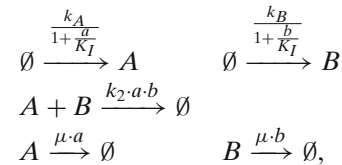
There is a bound in the theorem on the difference between the solution of the master equation and the discretized FPE for interpolating functions depending on the discretization error  $\tau_{\text{FP}}$  for the FPE, how well the FPE approximates the master equation  $\tau_m$ , the deviation from zero of the space operator for the master equation  $|\Gamma_m(p_m)|_\infty$  for  $p_m$ , and the deviation from zero of the discretization of the FPE in space and time  $|\Gamma_{\text{FP}}(p_{\text{FP}})|_\infty$  for  $p_{\text{FP}}$ . If the third derivatives of  $q_r$  are all small, then the modeling error  $\tau_m$  in Lemma 1 will be small. The discretization error  $\tau_{\text{FP}}$  can be reduced by taking shorter time steps, using a finer grid, and by raising the order of the approximation from two. Both  $|\Gamma_m(p_m)|$  and  $|\Gamma_{\text{FP}}(p_{\text{FP}})|$  are zero at the grid points of their respective grids and  $|\Gamma_m(p_m)|_\infty$  and  $|\Gamma_{\text{FP}}(p_{\text{FP}})|_\infty$  are small for many  $p_m$  and  $p_{\text{FP}}$ . By taking  $\Omega$  to be in the interior of  $\mathbb{R}_+^N$  we can expect all  $w_r$  to be non-zero, so that Lemma 2 is satisfied.

## 5 Test problems

The test problems for the two algorithms in Sects. 2 and 3 are all systems with stiff behavior in the sense that they contain very different time scales as is common in biology. Lower case letters denote the copy numbers of the chemical species denoted by the upper case letter, e.g.  $a$  is the number of  $A$  molecules. In all models the biological cell volume is kept constant and cell growth is modeled by dilution, which takes the form of a constitutive degradation rate. Furthermore, the cell volumes are assumed to be well-stirred.

### 5.1 Two metabolites

Two metabolites,  $A$  and  $B$ , are consumed in a bimolecular reaction by rate  $k_2$  and degraded by rate  $\mu$ . The two metabolites are each synthesized by an enzyme. Both the synthesis rates are constrained by competitive inhibition [12] by the respective products. The dissociation constant of the product-enzyme complex  $K_I$  determines the strength of the product inhibition. We use two different inhibition strengths and call them “weak” and “strong”, see below. The reactions are:



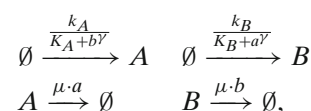
where  $k_A = k_B = 600 \text{ s}^{-1}$ ,  $k_2 = 0.001 \text{ s}^{-1}$ ,  $\mu = 0.0002 \text{ s}^{-1}$ . For weak inhibition  $K_I = 10^6$  and for strong inhibition  $K_I = 10^5$ . The computational domain is  $\Omega_h = [0, 3999] \times [0, 3999]$ . This case corresponds to the following parameters and functions in Sect. 2:

$$\begin{aligned} R &= 5, \mathbf{x}^T = (a, b), \\ w_1(\mathbf{x}) &= k_A / (1 + x_1 / K_I), \mathbf{n}_1^T = (-1, 0), \\ w_2(\mathbf{x}) &= k_B / (1 + x_2 / K_I), \mathbf{n}_2^T = (0, -1), \\ w_3(\mathbf{x}) &= k_2 x_1 x_2, \mathbf{n}_3^T = (1, 1), w_4(\mathbf{x}) = \mu x_1, \mathbf{n}_4^T = (1, 0), \\ w_5(\mathbf{x}) &= \mu x_2, \mathbf{n}_5^T = (0, 1). \end{aligned}$$

For some analysis of similar models in a biological context, see [8].

### 5.2 Toggle switch

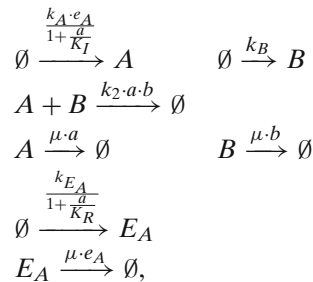
Two mutually cooperatively repressing gene products  $A$  and  $B$  can form a toggle switch. By binding to control sequences of the  $B$ -gene,  $A$  can inhibit production of  $B$  and vice versa. If  $A$  becomes abundant the production of  $B$  is inhibited and the system is in a stable state of high  $A$  and low  $B$ . If for some reason the amount of  $A$  falls or the amount of  $B$  is sufficiently high, the switch might flip and  $B$  becomes abundant and  $A$  will be repressed. This motif has been implemented in vivo in a cell [14]. In this model  $A$  and  $B$  are formed with maximal rates  $k_A/K_A$  and  $k_B/K_B$ , respectively. The parameters  $K_A$  and  $K_B$  determine the strength of the repression and  $\gamma$  is the degree of cooperativity of the repressive binding. The reactions are:



where  $k_A = k_B = 3 \times 10^3 \text{ s}^{-1}$ ,  $K_A = K_B = 1.1 \times 10^4$ ,  $\gamma = 2$  and  $\mu = 0.001 \text{ s}^{-1}$ . The computational domain is  $\Omega_h = [0, 399] \times [0, 399]$ .

### 5.3 Two metabolites and one enzyme

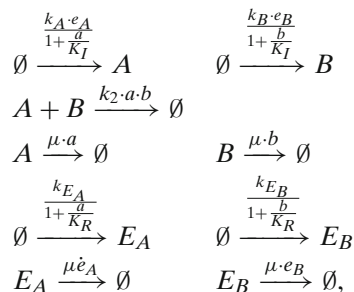
Test problem 5.1 is extended to three dimensions by a variable for the enzyme  $E_A$  that synthesizes metabolite  $A$ . The synthesis of the enzyme is controlled by a repression feedback loop [7]. The strength of the repression is determined by the constant  $K_R$ , which is a measure of the affinity of the repressor for the control site. The maximal rate of synthesis is given by the constant  $k_{E_A}$ . The reactions are:



where  $k_A = 0.3 \text{ s}^{-1}$ ,  $k_B = 1 \text{ s}^{-1}$ ,  $K_I = 60$ ,  $k_2 = 0.001 \text{ s}^{-1}$ ,  $\mu = 0.002 \text{ s}^{-1}$ ,  $K_R = 30$  and  $k_{E_A} = 0.02 \text{ s}^{-1}$ . The computational domain is  $\Omega_h = [0, 99] \times [0, 99] \times [0, 19]$ .

### 5.4 Two metabolites and two enzymes

Test problem 5.3 is extended by a variable for the enzyme  $E_B$  that synthesizes metabolite  $B$  in the same way as  $E_A$  synthesizes  $A$ . The reactions are:



where  $k_A = k_B = 0.3 \text{ s}^{-1}$ ,  $k_2 = 0.001 \text{ s}^{-1}$ ,  $K_I = 60$ ,  $\mu = 0.002 \text{ s}^{-1}$ ,  $k_{E_A} = k_{E_B} = 0.02 \text{ s}^{-1}$  and  $K_R = 30$ . The computational domain is  $\Omega_h = [0, 99] \times [0, 99] \times [0, 19] \times [0, 19]$ .

## 6 Numerical results

In this section, the numerical method for solution of the FPE in (3) approximating the master equation in (2)

in Sect. 2 and the Stochastic Simulation Algorithm in Sect. 3 for the master equation are applied to the four different systems in Sect. 5. The domain  $\Omega_h$  is covered by a grid with a constant step size  $h$ . A grid adapted to the solution as in [25] would improve the performance of the FPE solver. The execution time to compute solutions of equal accuracy is compared on a Sun server (450 MHz UltraSPARC II) and the procedures to estimate the solution errors and the variance in SSA are verified.

### 6.1 Error estimation in 1D

For simple one-dimensional systems there are exact solutions to the master equation and the FPE. One such simple system is this 1D birth-death process:



The birth rate  $k$  and the death rate  $q$  determine the first moment of the distribution  $\lambda = k/q$ . The exact solution to the master equation is a Poisson distribution

$$p_m(a) = e^{-\lambda} \frac{\lambda^a}{a!}, \tag{29}$$

where  $a \in \mathbb{Z}_+$ . The exact solution of the FPE approximation is [22]

$$p_{\text{FP}}(a) = C e^{-2a} \left(1 + \frac{a}{\lambda}\right)^{4\lambda-1}, \tag{30}$$

where  $a \in \mathbb{R}_+$  and  $C$  is a scaling constant such that  $\int_0^\infty p_{\text{FP}}(x) dx = 1$ .

The error  $e_v$  in the solutions computed by SSA and FPE is determined using the exact PDFs  $p_m$  in (29) and  $p_{\text{FP}}$  in (30) and compared with the estimated error according to Sects. 3.2 and 2.4 for three different  $\lambda$  in Figure 1.

Ideally, the symbols in Fig. 1 should coincide with the reference line but the estimate in the SSA case is at most wrong with a factor 2 and the estimate for the FPE is asymptotically correct when the estimate tends to zero.

### 6.2 Modeling error

In Sect. 4, the difference between the solutions of the master equation (2) and the discretized FPE (12) depends on two quantities: the modeling error  $\tau_m$  and the discretization error  $\tau_{\text{FP}}$ . The difference  $e_m(j) = p_{\text{FP}}(j) - p_m(j)$  due to the modeling is computed for  $j = 0, 1, \dots, 2\lambda$ , and three  $\lambda$ -values in (30) and (29). The result measured in the  $\ell_1$ -norm is found in Table 1. The deviation from the master solution is small.

**Fig. 1** The true errors  $\|e\|_1$  in the SSA solution (*left*) and the FPE solution (*right*) are compared to the estimated error

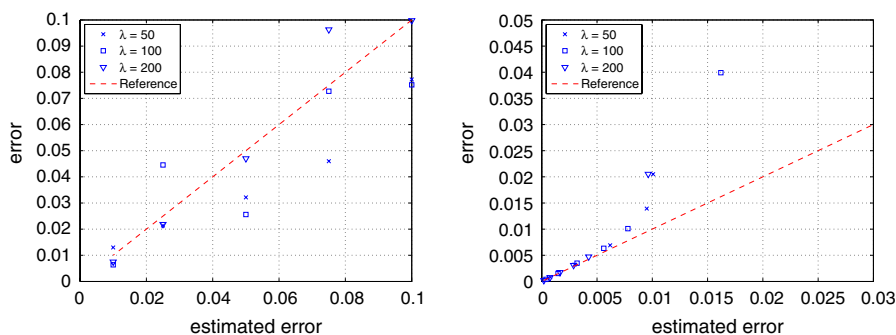


**Table 1** The FPE approximation error

$\lambda$	50	100	500
$\ e_m\ _1$	$1.18 \times 10^{-3}$	$5.88 \times 10^{-4}$	$1.17 \times 10^{-4}$

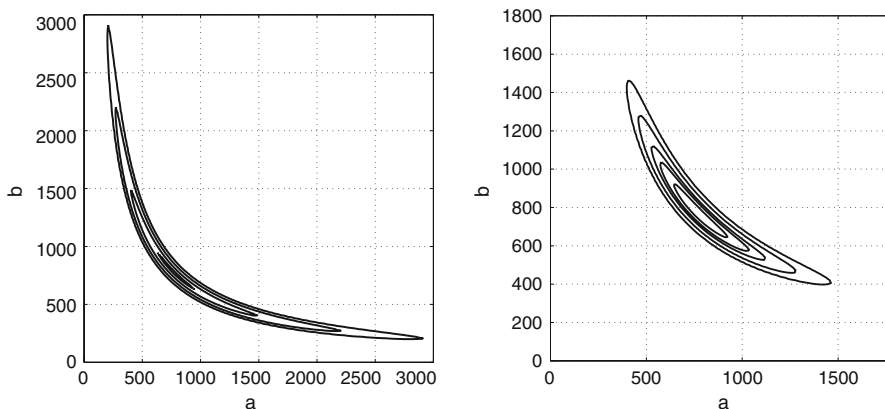
**Table 2** Two metabolites, weak inhibition, approximation error

Computational cells	$\epsilon$	$\ p_{FPE} - p_{SSA}\ _1$
$170 \times 170$	0.122	0.159
$180 \times 180$	0.0690	0.0583
$190 \times 190$	0.0480	0.0618
$200 \times 200$	0.0368	0.0636
$300 \times 300$	0.0128	0.0499

Exact solutions with two or more chemical species are known only in special cases. Instead, we compare the computed PDFs  $p_{FPE}$  and  $p_{SSA}$  at the steady state obtained with the FPE and the SSA for the system in Sect. 5.1 with weak inhibition. Five different grids with different error tolerances  $\epsilon$  are compared in Table 2.

By changing the grid size,  $\tau_{FP}$  in the theorem in Sect. 4 is changed but the modeling error  $\tau_m$  remains the same. We infer from the table that for high tolerances the discretization error dominates, while for a low  $\epsilon$  the difference in  $p$  is explained by the modeling error.

**Fig. 2** The steady state solutions of the 2D examples with weak (*left*) and strong (*right*) inhibition



### 6.3 Two-dimensional systems

The FPE solution and the SSA solution of three 2D problems are computed with the same estimated accuracy following Sects. 2.4 and 3.2. The execution times are compared for the two algorithms to calculate the steady state and the time-dependent solutions. The execution time includes discretization and computation of the solution. For the steady state problem in 1D–3D the Arnoldi method is used for computation of eigenpairs, in 4D the Jacobi–Davidson method is used instead. The error estimation is not included in the execution time.

The first example is the problem with two metabolites and weak inhibition in Sect. 5.1. The isolines of the steady state solution are found in Fig. 2. The work to reach steady state,  $W_{FPE}$  and  $W_{SSA}$ , is measured in seconds for the two algorithms and different number of cells and estimated errors  $e$  and is found in Table 3. Remember that with a stricter 95 % confidence interval for the error in SSA the computational times would be about four times longer.

The estimated  $\sigma$  for the same problem using  $\Delta\tau = 5 \times 10^3$ , the final time  $T_{max}$  in (19), the number of events in SSA  $N_{evt}$ , and the computational time  $t_\sigma$  in seconds to determine  $\sigma$  are shown in Table 4 for the same grids as in Table 3. The estimates of  $\|\sigma\|_1$  are stable independent of the grid size. The work to calculate  $\sigma$  is considerable

**Table 3** Computational work in seconds for the steady state solution of the test problem with two metabolites and weak inhibition value

Cells	$\ e\ _1$	$W_{FPE}$	$W_{SSA}$
170 × 170	0.122	194	$1.25 \times 10^3$
180 × 180	0.0690	207	$4.64 \times 10^3$
190 × 190	0.0480	229	$1.22 \times 10^4$
200 × 200	0.0368	254	$1.84 \times 10^4$
300 × 300	0.0128	584	$1.04 \times 10^5$
350 × 350	0.00920	793	$2.26 \times 10^{5*}$

The time marked with \* is an estimated

**Table 4** Parameters in the SSA computation of the steady state solution of the test problem with two metabolites and weak inhibition

Cells	$\ \sigma\ _1$	$T_{max}$	$N_{evt}$	$t_\sigma$
170 × 170	0.941	$2.98 \times 10^5$	$5.35 \times 10^8$	2,350
180 × 180	0.941	$9.30 \times 10^5$	$1.67 \times 10^9$	3,190
190 × 190	0.940	$1.92 \times 10^6$	$3.45 \times 10^9$	3,180
200 × 200	0.900	$2.92 \times 10^6$	$5.25 \times 10^9$	2,550
300 × 300	0.909	$2.52 \times 10^7$	$4.54 \times 10^{10}$	2,490
350 × 350	0.964	$5.49 \times 10^7$	$9.87 \times 10^{10}$	2,440

**Table 5** Determination of  $\Delta\tau$  for  $\sigma$  estimation in the SSA computation of the steady state solution of the test problem with two metabolites and weak inhibition

$\Delta\tau$	$T_{max}$	$\ \sigma\ _1$	$t_\sigma$
$5 \times 10^1$	$2.07 \times 10^5$	3.80	21.2
$5 \times 10^2$	$7.86 \times 10^5$	1.98	203
$5 \times 10^3$	$1.72 \times 10^6$	0.928	2,030
$5 \times 10^4$	$2.12 \times 10^6$	0.326	20,400

compared to the work for the full simulation  $W_{SSA}$  for the small problems but is negligible for the large problems. The number of events in the SSA is almost  $10^{11}$  for the largest grid.

The parameter  $\Delta\tau$  is determined by numerical experiments for one grid and is assumed to be valid for all space discretizations. In Table 5 we show  $T_{max}$  in (19),  $\|\sigma\|_1$ , and the computational time  $t_\sigma$  to determine  $\sigma$ . Between  $\Delta\tau = 5 \times 10^3$  and  $5 \times 10^4$ ,  $\|\sigma\|_1$  drops at the expected rate and  $T_{max}$  stabilizes.

Table 6 contains the results for the steady state solution of the same system with strong inhibition. The steady state solution is plotted in Fig. 2.

The execution times for computing the steady state solution and the time-dependent solution at  $T = 10^4$  for the toggle switch in Sect. 5.2 are collected in Tables 7 and 8. The initial solution at  $t = 0$  is a Gaussian distribution  $\mathcal{N}(\mu, \sigma^2)$  with  $\mu = (133, 133)^T$  and  $\sigma_j^2 = \mu_j$ . The number of trajectories  $L$  generated to achieve the same

**Table 6** Computational work for the steady state solution of the test problem with two metabolites and strong inhibition

Cells	$\ e\ _1$	$W_{FPE}$	$W_{SSA}$
120 × 120	0.0944	95.1	$4.35 \times 10^2$
160 × 160	0.0478	168	$1.74 \times 10^3$
200 × 200	0.0263	268	$6.11 \times 10^3$
240 × 240	0.0172	414	$1.22 \times 10^4$
280 × 280	0.0130	545	$1.65 \times 10^4$
300 × 300	0.0115	667	$2.28 \times 10^4$
340 × 340	0.00898	849	$3.68 \times 10^4$

**Table 7** Computational work for the steady state solution of the toggle switch problem

Cells	$\ e\ _1$	$W_{FPE}$	$W_{SSA}$
30 × 30	0.134	4.91	$1.11 \times 10^2$
50 × 50	0.0355	9.93	$1.47 \times 10^3$
70 × 70	0.0208	19.7	$3.57 \times 10^3$
90 × 90	0.0129	33.2	$1.18 \times 10^4$
110 × 110	0.00832	50.1	$2.82 \times 10^4$

**Table 8** Computational work for the time-dependent solution of the toggle switch problem at  $T = 10^4$

Cells	$\ e\ _1$	$W_{FPE}$	$L$	$W_{SSA}$
30 × 30	0.0952	7.08	$7.8 \times 10^3$	$8.35 \times 10^1$
50 × 50	0.0339	18.1	$1.6 \times 10^5$	$1.68 \times 10^3$
70 × 70	0.0164	35.6	$1.3 \times 10^6$	$1.36 \times 10^4$
90 × 90	0.00979	61.9	$5.9 \times 10^6$	$6.25 \times 10^4$
110 × 110	0.00667	98.0	$1.9 \times 10^7$	$1.95 \times 10^5$

accuracy with SSA as in the PDE solution is more than  $10^7$  in some cases. The time evolution of a system with an unsymmetric initial distribution is displayed in Fig. 3.

The FPE solver is much faster than the SSA, especially for higher accuracies, in all the examples above. The difference is two orders of magnitude or more in many cases. This is explained by the work estimates in Sects. 2.5 and 3.2. For 2D problems and second order accuracy for the steady state solution, the work for the FPE based algorithm is proportional to  $\epsilon^{-1}$  but for SSA it is  $\propto \epsilon^{-2}$ .

### 6.4 Three-dimensional system

The work in seconds to compute the steady state solution of the test problem with three molecular species in Sect. 5.3 is found in Table 9. The execution times for the FPE are somewhat longer compared to problems of the same size in 2D in the previous section but the SSA is much faster making it the preferred algorithm.

**Fig. 3** A solution of the toggle switch at  $t = 10^3$  (left) and  $t = 10^6$  (right)

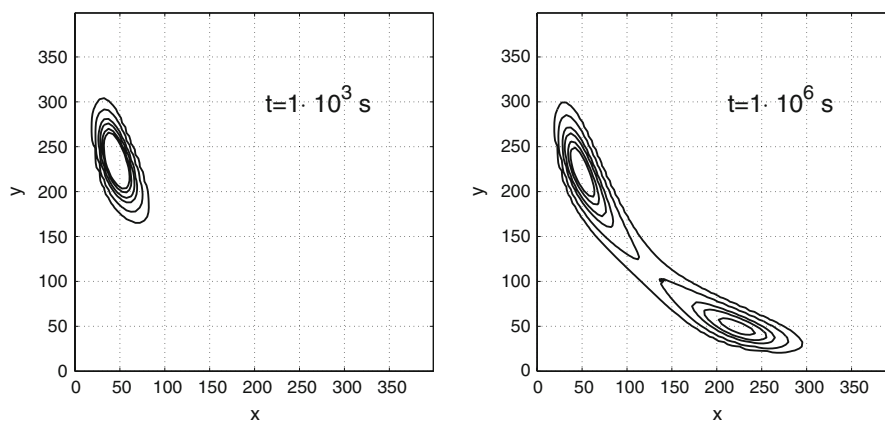


**Table 9** Computational work for steady state solution of the test problem with two metabolites and one enzyme

Cells	$\ e\ _1$	$W_{FPE}$	$W_{SSA}$
$18 \times 18 \times 18$	0.102	82.6	5.72
$20 \times 20 \times 20$	0.0859	121	10.4
$30 \times 30 \times 20$	0.0618	316	22.1
$40 \times 40 \times 20$	0.0565	658	33.6
$40 \times 40 \times 30$	0.0296	1740	124

The speed of the SSA for this problem is mainly due to the fact that molecule numbers are very small and the system is not very stiff. Since a trajectory is simulated the method is very dependent of both these properties. Still, the FPE has convergence properties that will make it useful for 3D problems.

### 6.5 Four-dimensional system

The methods for the steady state problem in Sect. 5.4 are compared in Table 10.

Also here SSA is much more efficient than the FPE based algorithm. This is what we can expect when the dimension of the problem increases.

The computational work for the time-dependent, four-dimensional problem at time  $T = 100$  is displayed in Table 11. The initial distribution is a Gaussian distribution  $\mathcal{N}(\mu, \sigma^2)$  with  $\mu = (33, 33, 7, 7)^T$  and  $\sigma_j^2 = \mu_j$ .

**Table 10** Computational work for the steady state solution of the test problem with two metabolites and two enzymes

Cells	$\ e\ _1$	$W_{FPE}$	$W_{SSA}$
$18 \times 18 \times 18 \times 18$	0.104	2,510	41.9
$20 \times 20 \times 20 \times 20$	0.0864	4,150	59.8
$24 \times 24 \times 24 \times 24$	0.0772	5,900	93.4
$30 \times 30 \times 20 \times 20$	0.0723	9,340	126

**Table 11** Computational work for the time-dependent solution at  $T = 100$  of the four-dimensional problem

Cells	$\ e\ _1$	$W_{FPE}$	$L$	$W_{SSA}$
$18 \times 18 \times 18 \times 18$	0.0930	$4.55 \times 10^3$	$1.0 \times 10^6$	$8.51 \times 10^2$
$20 \times 20 \times 20 \times 20$	0.0789	$6.26 \times 10^3$	$6.0 \times 10^5$	$1.48 \times 10^3$
$24 \times 24 \times 24 \times 24$	0.0547	$9.98 \times 10^3$	$4.1 \times 10^6$	$4.08 \times 10^3$
$30 \times 30 \times 20 \times 20$	0.0573	$1.29 \times 10^4$	$3.0 \times 10^6$	$5.63 \times 10^3$

The difference is smaller between the two solution methods for the 4D time-dependent case than for the steady state problem in Table 10. The explanation to this behavior is that the ergodic property of the system makes steady state solutions with SSA efficient since the entire simulated trajectory can be used to estimate the solution. The time-dependent solution of  $p$  is computed by simulation of trajectories in time where only the final state can be used for the solution. About  $10^6$  realizations by SSA are necessary for the same accuracy as in the FPE solution.

### 6.6 Execution time in theory and experiments

The predictions of the work estimates in Sects. 2.5 and 3.2 are compared to the recorded execution times in Figs. 4, 5, and 6. The agreement for the steady state problems is good in all cases except for the two metabolites with weak inhibition and the 3D problem in Fig. 4. However, for lower tolerances in the asymptotic regime the trend is as expected from (15) for all examples.

A faster growth of the work is predicted by (16) than is measured in Fig. 6 for the time-dependent problems. The maximum local error in the adaptive time discretization is allowed to be as large as the error in the space discretization. The initial time step is chosen to be  $\Delta t^0 = 0.01T$  and the growth in  $\Delta t$  in every step is limited. The result is that the maximum time step is not reached for any  $\epsilon$  and almost the same sequence of steps is generated in

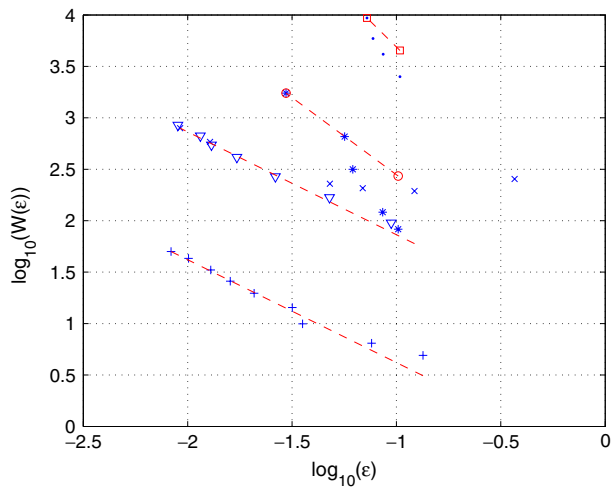


**Fig. 4** Work as a function of the tolerance  $\epsilon$  for the steady state problem solved by the FPE: 2D - weak inhibition (*cross*), 2D - strong inhibition (*inverted triangle*), toggle switch (*plus*), 3D (*asterisk*) and 4D (*dot*), and dashed reference lines with slopes  $-1$  (*no symbol*),  $-3/2$  (*open circle*) and  $-2$  (*open square*)

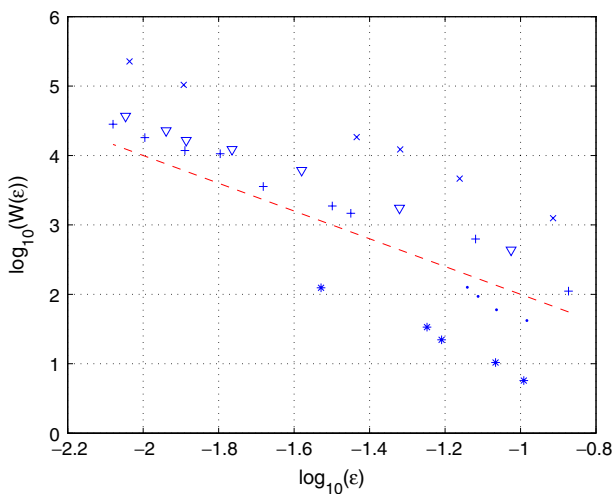


**Fig. 5** Work as a function of tolerance for the steady state problem solved by the SSA: 2D-weak inhibition (*cross*), 2D - strong inhibition (*inverted triangle*), toggle switch (*plus*), 3D (*asterisk*) and 4D (*dot*), and dashed reference line with slope  $-2$

all examples. Hence, the work is relatively independent of the time integration and is dominated by the space discretization as it is in the steady state problem.

## 7 Conclusions

Two methods to approximate the probability density function for the molecular copy numbers in biochemical reactions with a few molecular species have been derived and compared. The steady state solution and the

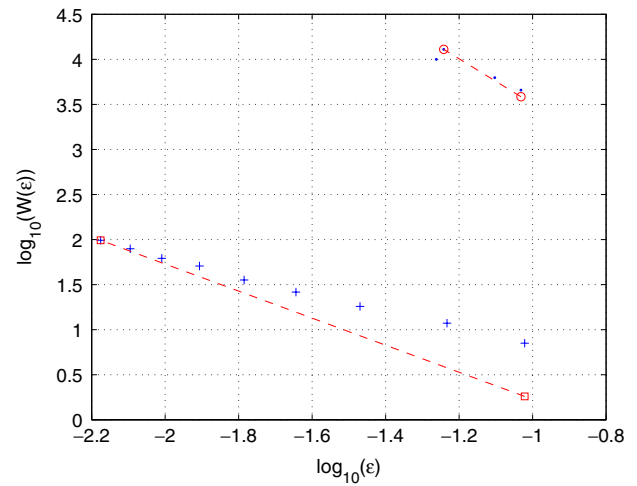


**Fig. 6** Work as a function of tolerance for the time-dependent problem solved by the FPE: toggle switch (*plus*) and 4D (*dot*), and dashed reference lines with slopes  $-3/2$  (*open square*),  $-5/2$  (*open circle*)

time-dependent solution of the Fokker–Planck equation (FPE) have been computed and the same solutions have been obtained by the Stochastic Simulation Algorithm (SSA) [16].

A bound on the difference between the solutions is proved by the maximum principle for parabolic equations. The errors in the numerical methods are estimated and the execution times for equal errors are compared. The FPE approach is much more efficient for the two-dimensional test problems while SSA is the preferred choice in higher dimensions. However, the results depend on the properties of the problem: the size of the computational domain, the stiffness of the chemical reactions, and the chosen error tolerance.

**Acknowledgments** Paul Sjöberg has been supported by the Swedish Foundation for Strategic Research, the Swedish Research Council, and the Swedish National Graduate School in Scientific Computing. Johan Elf has been supported by Måns Ehrenberg's grant in Systems Biology from the Swedish Research Council and the Knut and Alice Wallenberg Foundation. Johan Tysk provided us with [1].

## References

1. Aronson, D.G., Serrin, J.: Local behavior of solutions of quasi-linear parabolic equations. *Arch. Rat. Mech. Anal.* **25**, 81–122 (1967)
2. Benzer, S.: Induced synthesis of enzymes in bacteria analyzed at the cellular level. *Biochim. Biophys. Acta* **11**, 383–395 (1953)
3. Berg, O.G.: A model for the statistical fluctuations of protein numbers in a microbial population. *J. Theor. Biol.* **71**, 587–603 (1978)

4. Berg, O.G.: On diffusion-controlled dissociation. *J. Chem. Phys.* **31**, 47–57 (1978)
5. Cao, Y., Gillespie, D., Petzold, L.: Multiscale stochastic simulation algorithm with stochastic partial equilibrium assumption for chemically reacting systems. *J. Comput. Phys.* **206**, 395–411 (2005)
6. Dieudonné, J.: Foundations of modern analysis, Academic, New York (1969)
7. Elf, J., Berg, O.G., Ehrenberg, M.: Comparison of repressor and transcriptional attenuator systems for control of amino acid biosynthetic operons. *J. Mol. Biol.* **313**, 941–954 (2001)
8. Elf, J., Paulsson, J., Berg, O.G., Ehrenberg, M.: Near-critical phenomena in intracellular metabolite pools. *Biophys. J.* **84**, 154–170 (2003)
9. Elowitz, M.B., Surette, M.G., Wolf, P.-E., Stock, J.B., Leibler, S.: Protein mobility in the cytoplasm of *Escherichia coli*. *J. Bacteriol.* **181**, 197–203 (1999)
10. Érdi, P., Tóth, J.: Mathematical models of chemical reactions. Princeton University Press, Princeton (1988)
11. Ferm, L., Lötstedt, P., Sjöberg, P.: Conservative solution of the Fokker–Planck equation for stochastic chemical reactions. *BIT* (in press, 2006)
12. Fersht, A.: Structure and mechanism in protein science: a guide to enzyme catalysis and protein folding. W. H. Freeman & Co, New York (1998)
13. Gardiner, C.W.: Handbook of stochastic methods. Springer, Berlin Heidelberg New York (1985)
14. Gardner, T.S., Cantor, C.R., Collins, J.J.: Construction of a genetic toggle switch in *Escherichia coli*. *Nature* **403**, 339–342 (2000)
15. Gilbarg, D., Trudinger, N.S.: Elliptic partial differential equations of second order. Springer, Berlin Heidelberg New York (1977)
16. Gillespie, D.T.: A general method for numerically simulating the stochastic time evolution of coupled chemical reactions. *J. Comput. Phys.* **22**, 403–434 (1976)
17. Greenbaum, A.: Iterative methods for solving linear systems. SIAM, Philadelphia (1997)
18. Hairer, E., Nørsett, S.P., Wanner, G.: Solving ordinary differential equations, nonstiff problems. 2nd edn., Springer, Berlin Heidelberg New York (1993)
19. Haseltine, E.L., Rawlings, J.B.: Approximate simulation of coupled fast and slow reactions for stochastic chemical kinetics. *J. Chem. Phys.* **117**, 6959–6969 (2002)
20. John, F.: Partial differential equations. 3rd edn., Springer, Berlin Heidelberg New York (1980)
21. Kærn, M., Elston, T.C., Blake, W.J., Collins, J.J.: Stochasticity in gene expression: from theories to phenotypes. *Nat. Rev. Genet.* **6**, 451–464 (2005)
22. van Kampen, N.G.: Stochastic processes in physics and chemistry. Elsevier, Amsterdam (1992)
23. Larsen, R.J., Marx, M.L.: An introduction to mathematical statistics and its applications. 2nd edn., Prentice-Hall, Englewood Cliffs (1986)
24. Lehoucq, R.B., Sorensen, D.C., Yang, C.: ARPACK users' guide: solution of large-scale eigenvalue problems with implicitly restarted Arnoldi methods. SIAM, Philadelphia (1998)
25. Lötstedt, P., Söderberg, S., Ramage, A., Hemmingsson-Frändén, L.: Implicit solution of hyperbolic equations with space-time adaptivity. *BIT* **42**, 134–158 (2002)
26. MATLAB: The MathWorks, Inc., Natick, MA, USA, <http://www.mathworks.com>
27. Novick, A., Weiner, M.: Enzyme induction as an all-or-none phenomenon. *Proc. Natl. Acad. Sci. USA* **43**, 553–566 (1957)
28. Sleijpen, G.L.G., van der Vorst, H.A.: A Jacobi-Davidson iteration method for linear eigenvalue problems. *SIAM J. Matrix Anal. Appl.* **17**, 401–425 (1996)
29. van der Vorst, H.A.: Bi-CGSTAB: A fast and smoothly converging variant of Bi-CG for the solution of nonsymmetric linear systems. *SIAM J. Sci. Stat. Comput.* **13**, 631–644 (1992)
30. Xie, X.S.: Single-molecule approach to dispersed kinetics and dynamic disorder: Probing conformational fluctuation and enzymatic dynamics. *J. Chem. Phys.* **117**, 11024–11032 (2002)